AIAA SciTech Forum
23-27 January 2023, National Harbor, MD & Online
AIAA SCITECH 2023 Forum

10.2514/6.2023-1241

Summary of the Smooth Body Separation Test Case at the 2022 High Fidelity CFD Verification Workshop

Johan Larsson*
University of Maryland, College Park, MD 20742

Ivan Bermejo-Moreno†
University of Southern California, Los Angeles, CA 90089

Daniel Garmann‡ and Donald Rizzetta§
U.S. Air Force Research Laboratory, Wright-Patterson AFB, OH 45433

Robert Baurle
NASA Langley Research Center, Hampton, VA 23666

Timofey Mukha¶, Siavash Toosi‖, and Philipp Schlatter**
KTH Royal Institute of Technology, SE-100 44 Stockholm, Sweden

Christoph Brehm††, Sparsh Ganju‡‡ and Ali Berk Kahraman§§
University of Maryland, College Park, MD 20742

William van Noordt¶¶
University of Oxford, UK

Z. J. Wang***
University of Kansas, Lawrence, KS 66045

Zhaowen Duan†††
hiCFD, Lawrence, KS 66049

Marcel Blind‡‡‡ and Andrea Beck§§§
University of Stuttgart, Stuttgart, Germany

Sujal Dave¶¶¶ and Artem Korobenko[17]
University of Calgary, Calgary, AB T2N 1N4, Canada

*Associate Professor, Department of Mechanical Engineering, AIAA Associate Fellow.
†Assistant Professor, Department of Aerospace and Mechanical Engineering, AIAA Member.
‡Senior Research Aerospace Engineer, Aerodynamic Technology Branch, AIAA Associate Fellow.
§Senior Research Aerospace Engineer, Aerodynamic Technology Branch, AIAA Associate Fellow.
¶Postdoctoral Researcher, FLOW, Department of Engineering Mechanics.
‖Researcher, FLOW, Department of Engineering Mechanics.
**Professor, FLOW, Department of Engineering Mechanics.
††Associate Professor, Department of Aerospace Engineering, AIAA Member.
‡‡PhD student, Department of Aerospace Engineering, AIAA Member.
§§PhD Student, Department of Mechanical Engineering
¶¶PhD student, Department of Engineering Science, AIAA Member.
***Spahr Professor, Department of Aerospace Engineering, AIAA Fellow.
†††Research Engineer.
‡‡‡PhD student, Institute of Aerodynamics and Gas Dynamics.
§§§Professor, Department of Aerospace Engineering and Geodesy.
¶¶¶PhD student, Department of Mechanical and Manufacturing Engineering.
[17]Associate Professor, Department of Mechanical and Manufacturing Engineering, AIAA Member.

Wayne Strasser[18]
Liberty University, Lynchburg, VA

Rozie Zangeneh[19]
University at Buffalo, Buffalo, NY 14260

Stephen Guzik[20]
Colorado State University, Fort Collins, CO 80523

Sean Walters[21]
Southern Adventist University, Collegedale, TN 37315

Marshall Galbraith
Massachusetts Institute of Technology, Cambridge, MA 02139

The High Fidelity CFD Workshop was held on January 8-9, 2022, and covered a range of test cases focused on verification. The present paper contains a summary of the test case focused on smooth body separation prediction using wall-modeled large eddy simulation, to which 11 participant teams submitted blind predictions.

I. Introduction

This work started through discussions in the AIAA discussion group focused on large eddy simulations (LES) over the course of several years. These discussions kept coming back to the same question of how one asserts the quality of an LES. An earlier incarnation of the discussion group published a review paper on the state of LES and recommended practices [1]. In January 2018, the discussion group converged on the idea of doing a workshop focused on verification of a smooth-body separation flow using wall-modeled large eddy simulation (WMLES).

After considering possible test cases, it was decided to focus on a test case for which no experimental data existed. While unusual, this had the benefit of creating an atmosphere of non-competitive learning rather than an exercise in declaring a winner. This also makes the focus of the workshop be entirely on verification rather than validation, i.e., on questions like "is my code bug-free?", "is my grid sufficiently fine?", "is my inflow turbulence sufficiently developed?", and "does my outflow boundary condition affect the flow?".

The chosen test case is a version of the smooth ramp flow studied experimentally by Simmons et al. [2]. The flow in the experiment was highly three-dimensional; for the workshop it was decided to instead pursue simulations in a very narrow spanwise periodic domain in order to make the simulations more affordable. Affordability was considered key when designing the test case, as this enables greater numerical experimentation, most importantly to run simulations on a sequence of finer grids to investigate convergence. The basic flow is visualized in Fig. 1.

Eleven groups of participants submitted results for the workshop in January, 2022. A sub-set of the participants then took part in a virtual follow-up "mini-workshop" in July, 2022, in which some refined results or parametric studies were considered.

The objective of this paper is to document the main aspects of the workshop and to provide an overview or sample of the results. The objective is not a comprehensive or complete documentation or analysis of the results, but rather to provide an overview.

II. Test case definition

The geometry of the problem is sketched in Fig. 2. The shape of the smooth ramp is taken from the experiment of Simmons et al. [2] and is defined by

$$\frac{y}{L} = \frac{H}{L}\left[1 - 10\left(\frac{x}{L}\right)^3 + 15\left(\frac{x}{L}\right)^4 - 6\left(\frac{x}{L}\right)^5\right],$$

[18] Associate Professor, School of Engineering.
[19] Research Scientist, Center for Hybrid Rocket Exascale Simulation Technology (CHREST), AIAA member
[20] Assistant Professor, Department of Mechanical Engineering.
[21] Assistant Professor, Physics & Engineering.

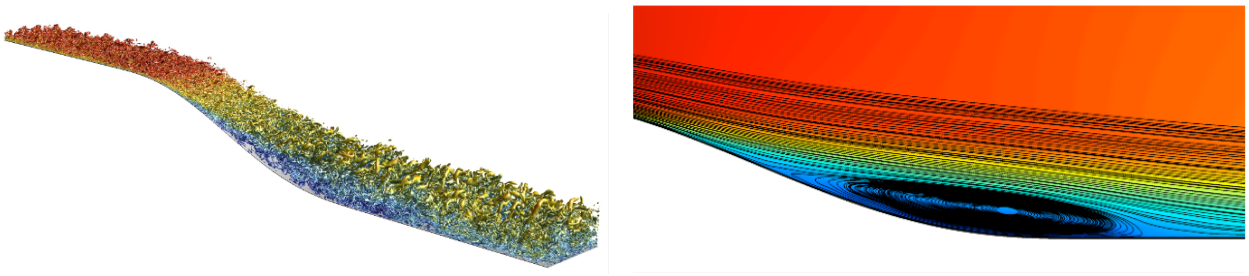

Fig. 1 Visualization of instantaneous turbulence and the mean streamlines.

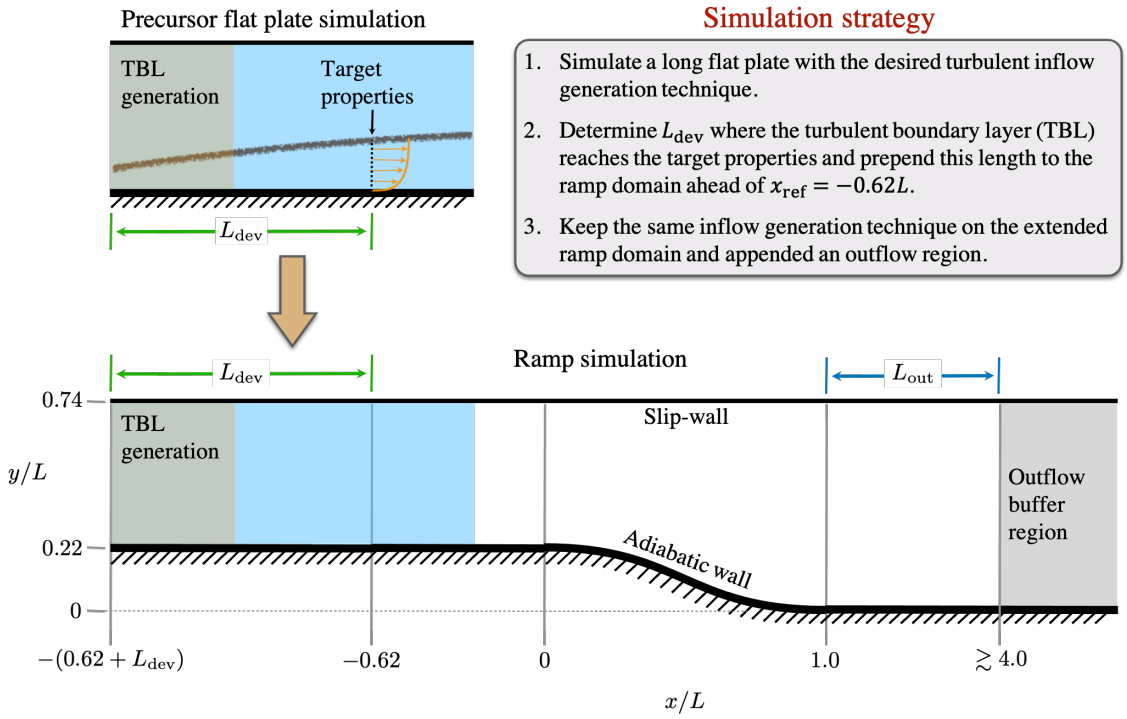

Fig. 2 Sketch of the computational domain and the recommended simulation strategy for how to choose the right inflow location to match the target properties at $x_{ref}/L = -0.62$.

where the ramp begins at $(x, y) = (0, H)$ and the height-to-length ratio of the ramp is $H/L = 0.22$. The top of the domain is an inviscid wall; this is preferred over a free upper boundary since it is easier to replicate in different codes. The spanwise domain width was set to a very narrow $L_z = 0.128L$. This choice was known to have a clear effect on the results, but with the thinking that every simulation should be affected similarly since a periodic boundary condition can be exactly represented in a code.

The problem specification leaves two important lengths to be chosen by each user. The outflow boundary condition generally has an unphysical effect some distance upstream of the outflow boundary, and therefore it is important to ensure that the outflow is placed sufficiently far downstream to minimize its effect on the region of interest. More generally, many codes/users use either a sponge (or buffer) region and/or a region of streamwise grid-stretching before the outflow, and then the relevant question is whether the beginning of this region (sponge and/or grid-stretching) begins sufficiently far downstream. The recommendation before the workshop was to start the outflow region no earlier than $x/L \approx 4$, meaning that the distance (in the sketch) $L_{out} \gtrsim 3$.

The idea of this test case is to assess the ability of the computational method to accurately predict the separated flow. To make comparisons between different simulations meaningful, it is therefore crucial that they have very similar incoming turbulent boundary layers. The target boundary layer thickness at $x_{ref} = -0.62L$ is $\delta_{ref} = 0.032L$, where

the boundary layer thickness δ is defined as the place where the mean velocity reaches 99% of the inviscid incoming flow velocity U_∞. Since different codes use different techniques to generate inflow turbulence, there is no way one can specify the "right" mean velocity profile at some upstream location. As a consequence, some degree of trial-and-error is essentially inevitable when trying to match the right boundary layer thickness at x_{ref}, *if* one only runs simulations in the smooth ramp domain. The recommended simulation strategy is to avoid the trial-and-error process by instead running a single simulation of a flat plate boundary layer with the inviscid upper wall (i.e., an extended version of the upstream portion of the smooth ramp domain) and to then identify where in this flat plate simulation the boundary layer best matches the target properties. If the distance from the inflow to the location where it matches the target properties is denoted by L_{dev}, the idea is to then use the same inflow boundary condition (mean profile, synthetic turbulence generation, etc) in the smooth ramp domain with the inflow placed exactly a distance L_{dev} upstream from the reference location x_{ref}. While this may at first seem to require additional work (an additional simulation without the ramp), it actually reduces the total amount of both human and computer time needed by removing the need for trial-and-error experimentation.

The Reynolds number of all cases computed at the workshop was $Re_L = 1.0 \cdot 10^6$, meaning $Re_\delta = 32{,}000$ based on the target boundary layer thickness at x_{ref}. Note that the boundary layer thickness was specified in terms of the 99% thickness rather than an integrated quantity to avoid discrepancies due to how the contribution from the wall-modeled layer was handled. The Mach number of the flow is nominally 0.2 based on the inviscid incoming velocity U_∞. At this small Mach number, minor variations in the actual mean pressure (which would change the actual Mach number) should have a negligible influence.

The workshop had a strong emphasis on investigating the grid sensitivity. To make it as simple as possible for participants to perform simulations on multiple grids, the organizers provided a sequence of grids ranging from very coarse to very fine. The main characteristics of the grids are illustrated in Fig. 3. The grids were designed by expert opinion without trying to create perfect grids. The streamwise and spanwise grid-spacings (Δx_s and Δz, respectively) were kept nominally equal over the ramp, with very gentle stretching towards a limiting state of $\Delta x_s \approx 2\Delta z$ in the upstream and downstream regions. The wall-normal grid-spacing Δx_n was chosen differently for wall-stress models and hybrid LES/RANS. For both types of grids, a sequence of grids with spanwise grid-spacing $\Delta z/\delta_{\text{ref}} = \{1/48, 1/32, 1/24, 1/16, 1/12, 1/8\}$ was created, with the streamwise grid-spacing Δx_s and the wall-normal grid-spacing Δx_n *away from the wall* refined by exactly the same ratios. The wall-normal grid-spacing *at* the wall was refined by less, to reduce the time step penalty in compressible codes with explicit time-stepping. Specifically, the grids suitable for wall-stress models used

$$\frac{\Delta x_{n,w}}{\delta_{\text{ref}}} = \frac{1}{80} + 0.3\left(\frac{\Delta z}{\delta_{\text{ref}}} - \frac{1}{48}\right).$$

For the grids suitable for hybrid LES/RANS, the first cell centroid was kept near $y_1^+ \approx 0.5$ in the incoming boundary layer.

III. Participants and methods

USC/UMD/KTH: Ivan Bermejo-Moreno (University of Southern California), Siavash Toosi (KTH, Sweden), Ali Berk Kahraman and Johan Larsson (both University of Maryland) used the `uPDE` code developed by Ivan Bermejo-Moreno. The code is an unstructured finite-volume code with nominally second-order accuracy and low-dissipation numerics. The Vreman subgrid model with original model coefficient of $C = 0.07$ was used. The standard equilibrium wall-model was used, with the exchange location taken as the closest cell centroid to a user-specified h_{wm} value (in most cases here, $h_{\text{wm}} = 0.1\delta_{\text{ref}} = 0.0032L$. The inflow turbulence was generated by a digital filtering method, with target Reynolds stress and imposed mean profiles taken from the auxiliary flat plate simulation at the finest grid level; i.e., the inflow specification was not adjusted for each grid. Numerical sponge layers with artificial dissipation (through an ENO scheme) were used near the top boundary (to help remove numerical noise) and towards the outflow boundary (to dampen outflow turbulence). The outflow sponge was started at $x/L = 3$ with the outflow boundary located at $x/L = 10$ for the base cases; these parameters were varied in separate runs. The workshop-provided grids were used throughout, but with a spanwise domain size of $L_z = 0.16L$ rather than the recommended $L_z = 0.128L$.

KTH/USC/UMD: The team members were the same as in the USC/UMD/KTH team, and used the same `uPDE` code with the same modeling choices. In contrast to the USC/UMD/KTH team, the grids were generated in a semi-automatic fashion as a way to experiment with structured grid-adaptation. Specifically, the LES residual estimator by Toosi and Larsson [3] was used to estimate where errors were created, and a genetic optimization method was used to find the best

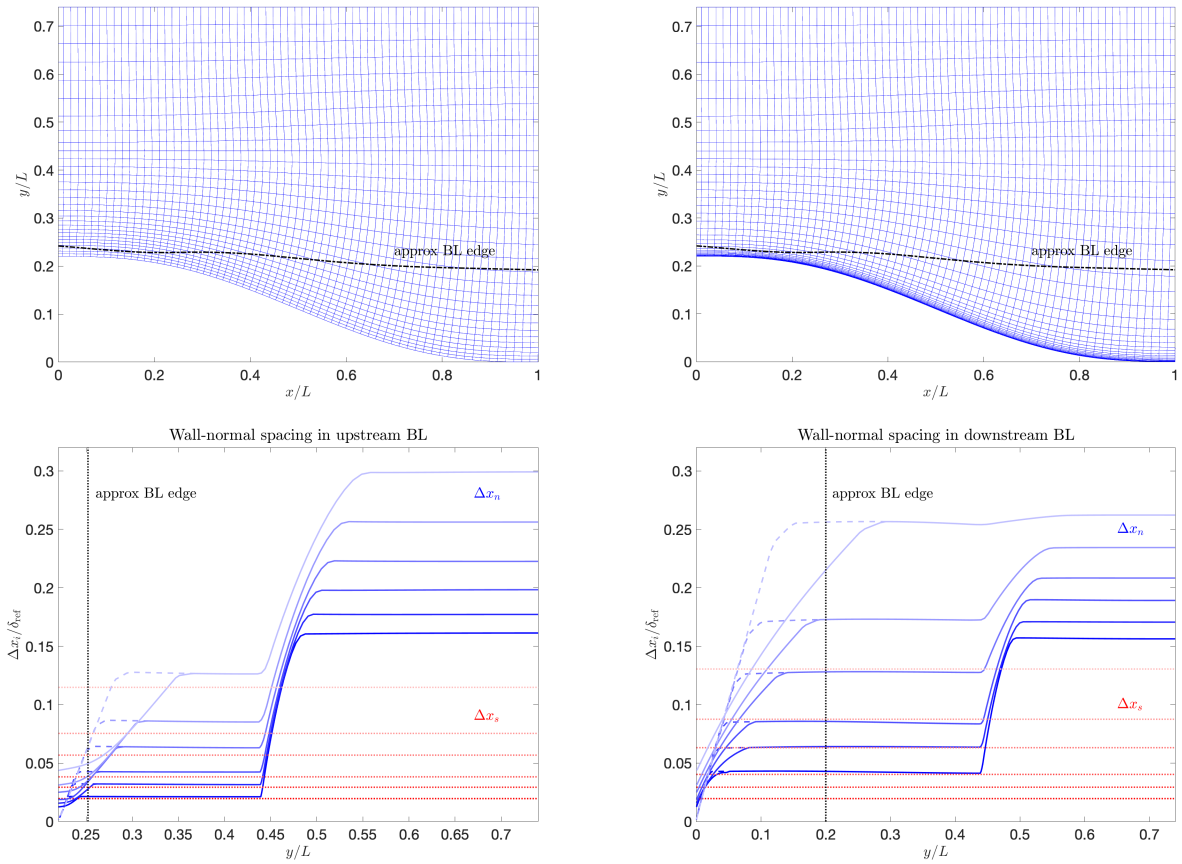

Fig. 3 The workshop-provided grids. Top row showing every 4th grid line on the coarsest grids for wall-stress models (left) and hybrid LES/RANS (right). Bottom row showing the wall-normal grid-spacing for the wall-stress models (solid lines) and hybrid LES/RANS (dashed lines), with the streamwise grid-spacing shown for reference (dotted red lines).

values of about $O(30)$ grid parameters to minimize the volume integrated residual field. For these grids, the correct spanwise domain size of $L_z = 0.128L$ was used,

AFRL: Dan Garmann and Don Rizzetta (Air Force Research Laboratory) used the `FDL3DI` sixth-order compact-finite-difference code with implicit modeling of the subgrid scales through an eighth-order-accurate spatial filter. The inflow turbulence was created by a transition strip shortly after the steady state inflow. This group pursued wall-resolved LES (WRLES), i.e., without a wall-model. Thus, meshes of higher resolution than the workshop grids were utilized. Details of the method, resolutions, and all results can be found in Rizzetta and Garmann [4].

KU/hiCFD: ZJ Wang (University of Kansas) and Duan Zhaowen (hiCFD) used the `hpMusic` high-order flux reconstruction code [5] with the Wall-Adaptive Local Eddy viscosity (WALE) subgrid model. This team ran on the same mesh but with different polynomial orders, p2 to p4, which produces the same effect as uniform refinement of the grid. The flow turbulence was generated by a cavity near the inlet boundary. The equilibrium wall-model obtains solution data from the 2nd element away from the wall [6]. In the p-refinement study, the wall-model data exchange location remains the same.

Calgary: Artem Korobenko and Sujal Dave (University of Calgary, Canada) used a variational multi-scale formulation for LES [7] with linear finite element (FEM) and quadratic NURBS discretization. The turbulent inflow was generated using synthetic turbulence generation (STG) method [8]. The turbulent eddies generated by STG are superimposed on benchmark average flow statistics from the DNS simulations [9] which are then applied as inlet boundary conditions.

The weakly-enforced Dirichlet boundary conditions were used at the wall [10] and traction-free boundary condition at the outflow with no sponge layer. Time integration was done using generalized-alpha method. The workshop-provided grids 6 to 4 were used for the analysis.

LTU: The LTU team was Rozie Zangeneh, currently at the University at Buffalo. The mesh was generated in the `OpenFOAM` solver. A hybrid LES-RANS model was used for wall modeling purposes. Improved Delayed Detached Eddy Simulation (IDDES) was deployed based on the $k-\omega$ SST model to compute the near-wall fields. The code was a compressible solver based on a second-order co-located scheme embedded in the `OpenFOAM` solver.

Liberty/Arkansas: Wayne Strasser (Liberty University) and Keith Walters (University of Arkansas) used the high-order spectral element Nek5000 v17.0 with a grid consisting of hexahedral elements. Simulations used polynomial orders $n = 7$, 11 and 15, resulting in these total DOFs: 4.6M (Coarse), 15.7M (Medium), and 37.2M (Fine). Aliasing was controlled by over-integration, and stability was ensured by filtering of the highest 25% wavenumber modes (max 5% damping). The constant coefficient Smagorinsky subgrid model with uniform filter size was used. Wall-modeling was applied in elements adjacent to the wall as follows: An analytical velocity profile was constructed as the sum of universal turbulent profile and a 2nd-order polynomial, with matching of the mean velocity and its wall-normal gradient at the first off-wall grid point Pseudo-flux terms were applied in the wall-modeling region to ensure mean velocity profile matches analytical profile. Finally, velocity boundary condition at wall were obtained by extrapolation from off-wall grid points (with imposed zero normal velocity). The inflow turbulence was generated using recycling from $x/L = -0.836$.

Stuttgart: Marcel Blind (University of Stuttgart, Germany) used the open source discontinuous Galerkin spectral element method (DGSEM) framework FLEXI which is developed at the University of Stuttgart. The simulations were run with $N = 7$ polynomials on Legendre-Gauss-Lobatto points using kinetic energy preserving split form fluxes according to Pirozzoli to mitigate aliasing instabilities [11]. Additionally, the Vreman subgrid model was used [12]. The inflow was generated using a combination of anisotropic linear forcing and a recycling rescaling approach (RRALF) [13]. An analytical equilibrium wall model based on Spalding's law of the wall was used. The interface location was set to 10% of the boundary layer thickness at the predefined target inflow location. The mesh was generated in-house using high-order curved elements with a geometric order of $N_{\text{geo}} = 4$.

KTH: Timofey Mukha and Philipp Schlatter (both KTH Royal Institute of Technology, Sweden) used `OpenFoam v1806`, which is an open-source code based on finite volume discretization. Uniform inflow was used, and volumetric forcing was applied in a small subset of near-wall cells downstream in order to trip the boundary layer. Spalding's law was used for wall modelling, and sampling was fixed to the second off-wall cell. The WALE model [14] was used for subgrid scale modeling. The grids provided by the workshop organizers were employed in the simulations. Linear interpolation was applied for computing both convective and diffusive cell-face fluxes. For time integration, a second-order backward-differencing scheme was used.

UMD/Oxford: Sparsh Ganju, Christoph Brehm (both University of Maryland) and William van Noordt (University of Oxford) used the higher-order Cartesian immersed boundary code CHAMPS. CHAMPS (Cartesian High-Fidelity Adaptive Multi-physics Solver) is a block-structured Cartesian solver employing adaptive mesh refinement (AMR) and a higher-order Immersed Boundary Method (IBM). It has been used in applications such as fluid-structure interactions, fluid-ablation-interactions, multiphase flows, wave-packet tracking and particle impingement for transition prediction, and wall-modeled large-eddy simulations for both low-speed and hypersonic flows. Inflow turbulence is generated using the digital filtering method, and the outflow pressure is set as a Dirichlet boundary condition at the freestream value while the other primitive variables are extrapolated. The no-slip wall and coupling between the IBM and the wall model used is as described in van Noordt et al.[15] The inviscid fluxes are computed using a second-order kinetic energy and entropy preserving scheme, and the viscous terms are evaluated using a second-order centered difference operator. Time integration is performed using a third-order strong-stability preserving Runge-Kutta scheme. More details about the numerical methods and schemes can be found in van Noordt et al.[15]

CSU: Stephen Guzik (Colorado State University) and Sean Walters (Southern Adventist University) used the CSU-developed structured finite-volume solver Chord for the tests [16]. The code was run at fourth-order accuracy for

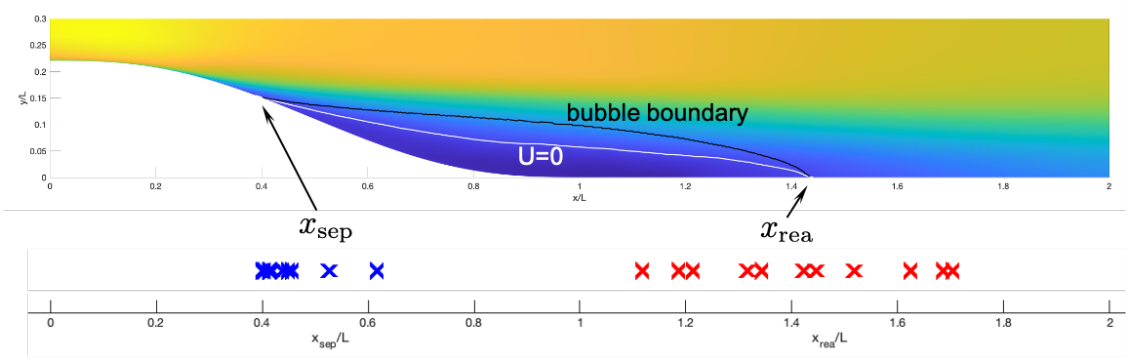

Fig. 4 Mean velocity with the bubble geometry and every participant's best prediction of the separation and reattachment locations.

spatial and temporal operations. Fixed adaptive mesh refinement provided de-refinement of the grid in the wall-normal direction away from the incoming boundary layer and the separation region. Additionally, the mesh was de-refined in the streamwise direction starting at three ramp-lengths downstream of the start of the ramp. The stretched-vortex model was used with the subgrid-scale vortex-direction model aligning with the eigenvector associated with the most positive eigenvalue of the strain-rate tensor. The stretched-vortex wall-model took information from the top of the wall-adjacent layer of cells to supply a slip-velocity boundary condition at the wall. The grid was generated from an analytical mapping to enable the use of multiblock, adaptive mesh refinement methods and to enable future exploration of the solution's mesh-dependence. The mapping was generated so as to closely match the wall-normal spacing of the near-wall region of the workshop mesh. From the wall-adjacent region, the mesh stretching did not reach the same intensity as the workshop generated mesh and so the final grid utilized was slightly more uniform in within the incoming boundary layer and the separation region.

IV. Inter-group comparisons

The smooth-ramp test case is aimed at testing the ability to predict a separated flow, and thus we focus here on a small subset of the results related to the separation bubble. The results are presented anonymously, labeling each participant A-K (not in the same order as in section III). However, we do note that participant A is a wall-resolved LES while the others are all wall-modeled LES.

A. Best case from each participant

Figure 4 shows a visualization of the mean separation bubble, both the separating streamline and the $U = 0$ contour that will be used later. The figure also shows the wide spread among the participants' predictions of the separation and reattachment locations x_{sep} and x_{rea}.

Figure 5 shows the friction coefficient c_f from each participant's best case, meaning their finest grid and their recommended baseline modeling choices. The ramp affects the boundary layer quite far upstream, as evidenced by the positive curvature of the friction coefficient c_f. The friction coefficient starts increasing around $x/L \approx -0.3$, suggesting an accelerated boundary layer at that point. The boundary layer then separates around $x_{\text{sep}}/L \approx 0.4 - 0.6$ in most of the results, and reattaches around $x_{\text{rea}}/L \approx 0.8 - 1.5$.

A different view of the separated flow region is shown in Fig. 6, which shows the locus of points where the mean streamwise velocity $U = 0$. Note that these lines are *not* the edge of the separation bubble, but rather cut through the separation bubble. Most participants predict a sizable separated region, with the exception of participants G and, to a lesser degree, I. In fact, participant G predicts a very strange second bubble which suggests a problem in the code or chosen models.

One hypothesis during the workshop discussions was that at least part of these differences could be traced to differences in the incoming flow. Figure 7 shows the boundary layer thickness in the incoming boundary layer for these cases. There is a large spread in values for δ_{99} at the reference location x_{ref}, ranging from about $0.025L$ to about $0.035L$. The large spread is almost certainly explained by the fact that very few participants actually followed the recommended procedure of running each case/grid first as a boundary layer to find the location where $\delta_{99} = 0.032L$ and then using

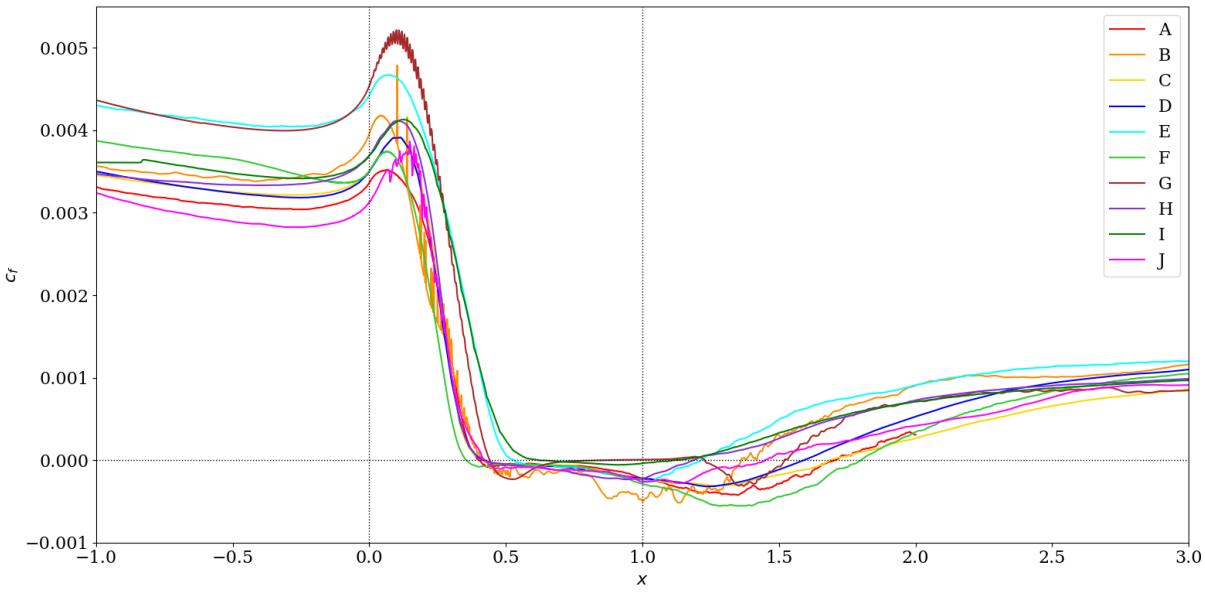

Fig. 5 Inter-group comparison of the friction coefficient as a function of the streamwise coordinate.

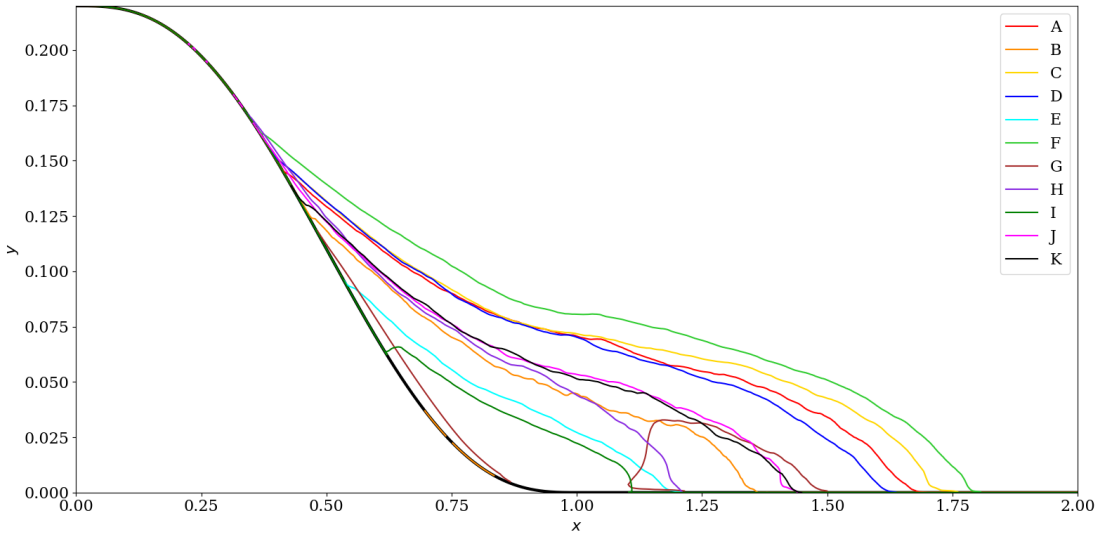

Fig. 6 Inter-group comparison of contours of zero mean streamwise velocity.

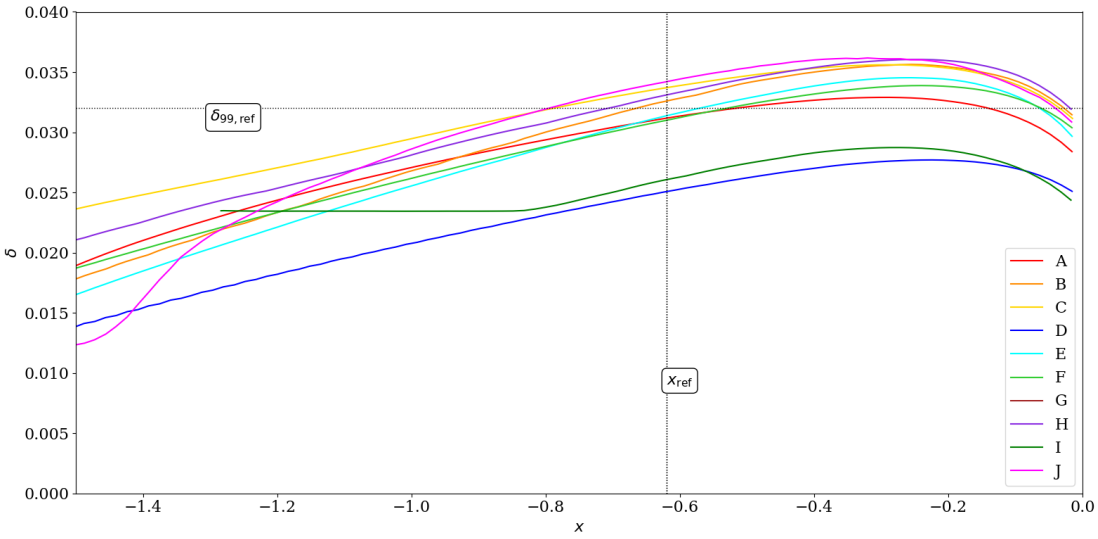

Fig. 7 Inter-group comparison of the boundary layer thickness (based on 99% of the freestream velocity) as a function of the streamwise coordinate.

exactly the same inflow specification and inflow location in the actual smooth ramp domain. Instead, participants generally tuned their inflow locations once for a specific grid and then used that for all other grids. In any case, there is no obvious connection between the incoming boundary layer thickness and the size of the separation bubble. For example, participants A, C, D and F show the largest bubbles, but they span almost the full range of δ_{99} values (A and F are in the middle, C is the second largest, D is the smallest).

Figure 8 shows the mean velocity profiles at both x_{ref} (incoming boundary layer) and $x = 0$ (the beginning of the ramp). It is again hard to see a trend here: for example, participant D has a fuller velocity profile than C and F, but all three lead to very similar sizes of the separation bubble.

B. Grid convergence

A major focus of this workshop is on how the results converge under grid refinement. There is a troubling habit in the LES community to refine the mesh until the results agree with experiments, but this is conceptually flawed – the correct simulation approach is to refine the mesh until the results no longer change, and only *then* to compare with experiment. It was therefore decided early on in the planning phase of this workshop that we would emphasize grid convergence. The organizers created 6 different grids differing in grid-spacing by a factor of 6 and in cell counts by almost a factor of 200.

Figure 9 shows the variation of the separation and reattachment locations with the grid size for each participant. Out of the 11 participants, 8 ran on multiple grids (or, in the case of high-order methods, on the same grid with globally different polynomial order).

The lack of any clear convergence trend is both surprising and sobering. The participants ran on grids with as few as 1 million to as many as 1.5 billion grid points, and yet there is no clear convergence or consensus of especially the reattachment location. There is arguably a trend for the separation location x_{sep} towards values in the range of $0.4L$ to $0.45L$ as one goes towards finer grids (rightwards in the figure).

The reattachment location x_{rea} generally increases (i.e., moves downstream) under grid-refinement. The results of participant D arguably shows some degree of convergence for the final two grids, but no other set of results show any real sign of convergence.

V. Discussion

The most surprising result in the workshop was the large spread in especially the reattachment location, both among the different participants and between different grids for any given participant. This should be taken as a sobering sanity

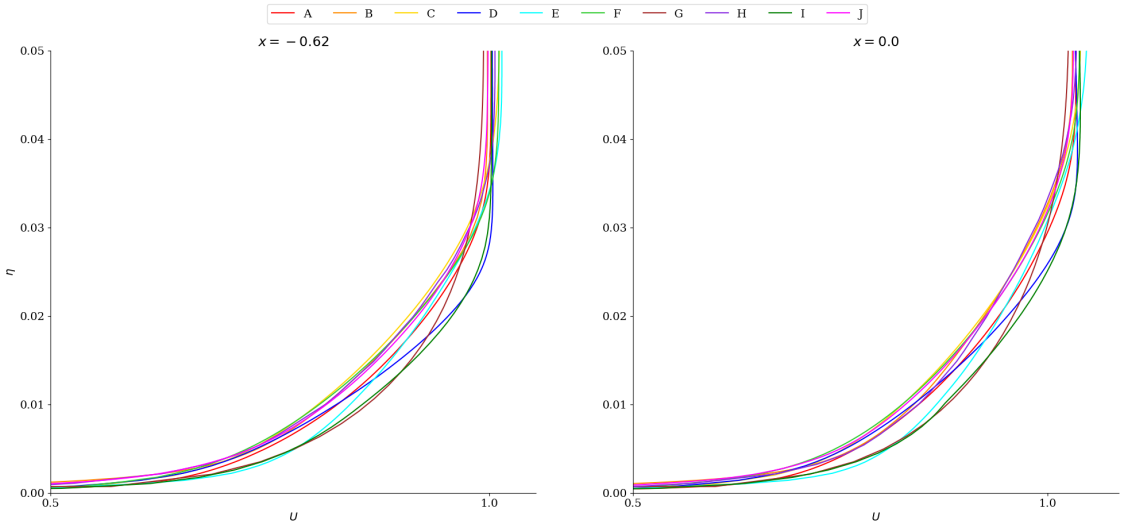

Fig. 8 Inter-group comparison of wall-normal profiles of mean streamwise velocity at the reference station ($x = -0.62$) (left) and at the start of the ramp ($x = 0$) (right).

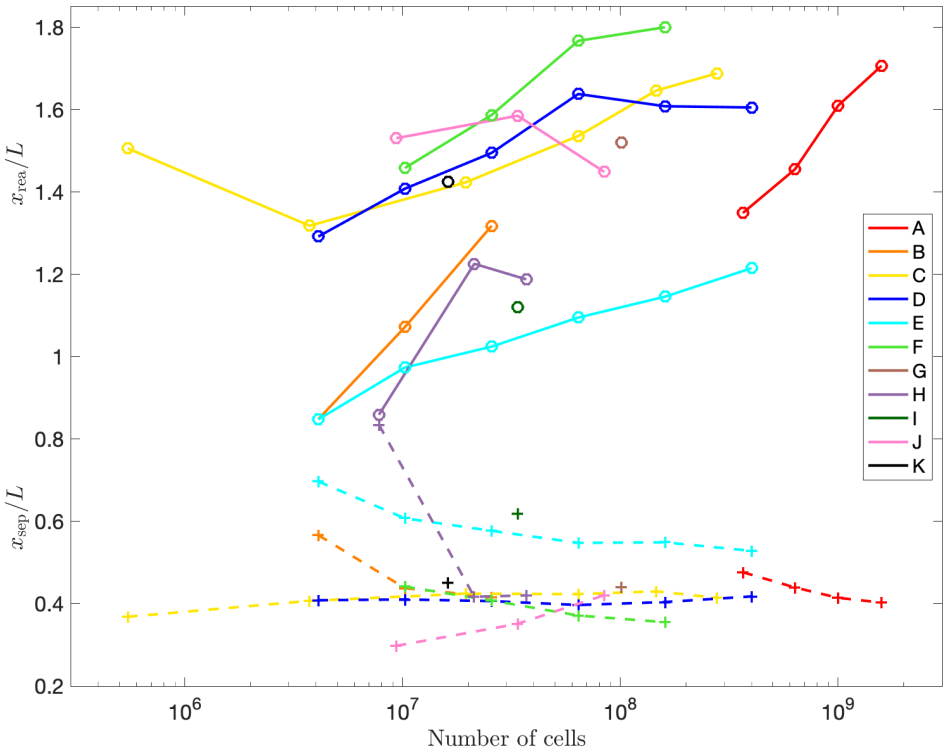

Fig. 9 Inter-group comparison of the separation (below, dashed lines) and reattachment (above, solid lines) locations.

check on how mature the wall-modeled LES technique really is. The fact that this workshop did NOT have any truth data (one participant performed wall-resolved LES, but the results were not shared with any participant prior to the workshop, and we collectively chose to not view those results as the surrogate truth) arguably helped bring this to light, by preventing participants from recognizing mistakes and issues needing attention before the actual workshop.

It is hard not to conclude that verification efforts in the WMLES arena, both code-verification and solution-verification, are important and need more attention.

It was hypothesized before and during the workshop that the incoming boundary layer, both its thickness and whether it had reached a fully developed turbulent state, would have a large effect on the separated flow. While no conclusion was reached, the evidence available during the workshop actually contradicts this hypothesis. First, participants A, C, D and F had very different incoming boundary layer thicknesses but produced similar-sized separation bubbles. Secondly, though not discussed in this paper, two participants varied the inflow location (which then affected both the thickness and developedness of the incoming boundary layer) and found very small changes in x_{sep} and x_{rea}. This question of how the upstream boundary layer affects the separated flow warrants additional attention and will be a focus of future workshops.

VI. Future workshops

The next High Fidelity CFD Verification workshop is scheduled for the Scitech 2024 meeting. Within the LES track of the workshop, the current plan is to consider 3 different test cases:

1) A flat plate boundary layer with an inviscid upper wall, i.e., the case used here to tune the inflow conditions. The 2022 workshop showed sufficiently large differences between different participants and different grid resolution levels to warrant a partial step backwards to a more canonical test problem, and the flat plate with an inviscid upper wall is the natural choice. The use of the inviscid upper wall matches the smooth ramp cases and removes the (minor) uncertainty introduced by having freestream conditions at the top boundary. We also note that the wall-modeled LES resource already contains comparisons for channel flow (`https://wmles.umd.edu/validation/channel-flow-at-re5200/`), which is arguably the most basic test case for WMLES.
2) The smooth ramp problem as investigated in 2022, with possible adjusted problem parameters.
3) An airfoil test case at the highest possible Reynolds number and at an angle-of-attack sufficiently large to produce a mildly separated flow. The exact details for this case are currently being decided and will be announced during Spring/Summer 2023.

Leading up to the 2024 workshop, the organizers and participants will continue the current pattern of monthly telecons in which we discuss problem specifications, investigations into specific questions, and other things. These telecons occur at 12:00 Eastern Time on the first Monday of every week, with details available at `https://wmles.umd.edu/workshops/workshop-2024`.

References

[1] Georgiadis, N. J., Rizzetta, D. P., and Fureby, C., "Large-eddy simulation: Current capabilities, recommended practices, and future research," *AIAA J.*, Vol. 48, No. 8, 2010, pp. 1772–1784. https://doi.org/10.2514/1.J050232.

[2] Simmons, D. J., Thomas, F. O., and Corke, T. C., "A smooth body, large-scale flow separation experiment," AIAA Paper 2018-0572, 2018.

[3] Toosi, S., and Larsson, J., "The Germano identity error and the residual of the LES governing equation," *J. Comput. Phys.*, Vol. 443, 2021, p. 110544.

[4] Rizzetta, D. P., and Garmann, D. J., "Wall-Resolved Large-Eddy Simulation of Smooth-Body Separated Flow," *Int. J. CFD*, Vol. 36, No. 1, 2022, pp. 1–22. https://doi.org/10.1080/10618562.2022.2087873.

[5] Wang, Z. J., Li, Y., Jia, F., Laskowski, G. M., Kopriva, J., Paliath, U., and Bhaskaran, R., "Towards industrial large eddy simulation using the FR/CPR method," *Comput. Fluids*, Vol. 156, 2017, pp. 579–589.

[6] Wang, Z. J., "High order wall-modeled large-eddy simulation on mixed unstructured meshes," *AIAA J.*, 2022. https://doi.org/10.2514/1.J061641.

[7] Bazilevs, Y., Calo, V., Cottrell, J., Hughes, T., Reali, A., and Scovazzi, G., "Variational multiscale residual-based turbulence modeling for large eddy simulation of incompressible flows," *Comp. meth. appl. mech. eng.*, Vol. 197, 2007, pp. 173–201.

[8] Shur, M. L., Spalart, P. R., Strelets, M. K., and Travin, A. K., "Synthetic turbulence generators for RANS-LES interfaces in zonal simulations of aerodynamic and aeroacoustic problems," *Flow Turb. Comb.*, Vol. 93, 2014, pp. 63–92.

[9] Schlatter, P., and Orlu, R., "Assessment of direct numerical simulation data of turbulent boundary layers," *J. Fluid Mech.*, Vol. 659, 2010, pp. 116–126.

[10] Bazilevs, Y., and Hughes, T., "Weak imposition of Dirichlet boundary conditions in fluid mechanics," *Comput. Fluids*, Vol. 36, 2007, pp. 12–26.

[11] Pirozzoli, S., "Generalized conservative approximations of split convective derivative operators," *Journal of Computational Physics*, Vol. 229, No. 19, 2010, pp. 7180–7190. https://doi.org/10.1016/j.jcp.2010.06.006.

[12] Vreman, A. W., "An eddy-viscosity subgrid-scale model for turbulent shear flow: Algebraic theory and applications," *Phys. Fluids*, Vol. 16, No. 10, 2004, pp. 3670–3681.

[13] Kempf, D., and Munz, C.-D., "Zonal direct-hybrid aeroacoustic simulation of trailing edge noise using a high-order discontinuous Galerkin spectral element method," *Acta Acust.*, Vol. 6, 2022, p. 39. https://doi.org/10.1051/aacus/2022030.

[14] Nicoud, F., and Ducros, F., "Subgrid-scale stress modelling based on the square of the velocity gradient tensor," *Flow Turb. Comb.*, Vol. 62, 1999, pp. 183–200.

[15] van Noordt, W., Ganju, S., and Brehm, C., "An immersed boundary method for wall-modeled large-eddy simulation of turbulent high-Mach-number flows," *J. Comput. Phys.*, Vol. 470, 2022, p. 111583. https://doi.org/https://doi.org/10.1016/j.jcp.2022.111583.

[16] Walters, S. P., "Large-eddy simulation of compressible flows using the stretched-vortex model and a fourth-order finite volume scheme on adaptive grids," Ph.D. dissertation, Colorado State University, 2022.